Article scientifique   Article   2005   Published version   Open Access

– –

Lattice Boltzmann Simulations of Blood Flow: Non-Newtonian Rheology and Clotting Processes

– –

Ouared, Mohamed Rafik; Chopard, Bastien

Lattice Boltzmann Simulations of Blood Flow: Non-Newtonian Rheology and Clotting Processes

Rafik Ouared[1] **and Bastien Chopard**[1]

The numerical simulation of thrombosis in stented aneurysms is an important issue to estimate the efficiency of a stent. In this paper, we consider a Lattice Boltzmann (LB) approach to bloodflow modeling and we implement a non-Newtonian correction in order to reproduce more realistic flow profiles. We obtain a good agreement between simulations and Casson's model of blood rheology in a simple geometry. Finally we discuss how, by using a passive scalar suspension model with aggregation on top of the LB dynamics, we can describe the clotting processes in the aneurysm.

1. INTRODUCTION

Numerical simulations offer a promising way to investigate bloodflow in complex situations. Recently, the Lattice Boltzmann (LB) method[8,30] has proved to be a flexible and powerful bloodflow solver.[4,13,18,19] In this paper we are interested in the case of modeling bloodflow in aneurysm and to describe the effect of placing a stent in the damaged parent vessel.

The first use of stents[2] in aneurysm treatments have been proposed in 1994[25,31] but it is only recently that neuro-surgeons started to use this technique in the reduction of intracranial aneurysms that affect large segments of the population, in their forties or older. About five to eight in 10, 0000 of western populations end up with an aneurysm rupture causing *subarachnoid haemorrhage (SAH)* every year, that can be lethal.[16]

---

[1]Computer Science Department, University of Geneva, 24 rue General-Dufour, CH-1211 Geneva 4, Switzerland; e-mail: bastien.chopard@cui.unige.ch
[2]The tubular mesh made of stainless steel or alloys.

209

Before stents, procedures like heavy by-pass surgery or slightly-invasive endovascular intervention with soft platinum coils occluding the aneurysms have been widely used and continue to be used with mitigated success, efficacy, and safety. Although no reliable intracranial aneurysms follow-up results are available today, the stents are subject to intensive study worldwide to optimize its efficacy and safety in the treatment of cerebral aneurysmal diseases.

As illustrated in ref. 19, it is admitted that stents reduce the blood-flow within the aneurysm and thus triggers the coagulation formation therein.[23] As a result, the aneurysm stops growing in volume and stops the rupture countdown as long as it is occluded by the *thrombus*. The efficiency of stent treatment depends on several parameters which are the object of intensive numerical simulations and experimental programmes.[1,6,15,17,18,21,24,29,33] The velocity reduction in the aneurysm resulting from the presence of the stent has been proposed as a first indicator of its efficiency. As shown in refs. 18 and 19, velocity reduction relies on both the geometry of the aneurysm and the structure design of the stent along with its positioning inside the parent vessel.

Blood clotting is an other way of measuring stent efficiency since it is the key to the aneurysm self-repair. Clotting is sensitive to the red blood cells behavior, hence to the non-Newtonian features of the blood.[14] Indeed, the blood clotting process, clinically observed in stented aneurysms, reveals the strong dependency of the increase of viscosity with small shear-rate flows.

The main goal of this paper is to propose a non-Newtonian extension to the standard LB model that incorporates correct blood rheology in case of small shear stress. In Section 3, we implement the so-called Casson's rheological model and compare LB simulation with the analytical velocity profile in a channel flow. In Section 4, we propose another extension whose purpose is to model the dynamics of clotting. Our approach is based on the transport by the plasma of red blood cells as well as an aggregation process starting in the low shear stress regions, near the aneurysms walls or stents struts. Next section starts with a short review of LB fluids and gives the relation between the shear stress and the strain rate. Finally, some conclusion are drawn in Section 5.

2. THE LATTICE BOLTZMANN METHOD

The lattice Boltzmann (LB) method is a rather new numerical technique aimed at modeling a physical system in terms of the dynamics of fictitious particles.[8,30] This method is now considered as a serious

alternative to standard computational fluid dynamics and has been widely used for simulating various complex fluid flows.

The main idea of the LB approach is to model the physical reality at a mesoscopic level: the generic features of microscopic processes can be expressed through simple rules, from which the desired macroscopic behavior emerges as a collective effect of the interactions between the many elementary components. An interesting advantage of the LB approach is their numerical simplicity and the ease to add new physical processes in the model. Furthermore their implementation on a parallel computer is straightforward.

In a LB model, a fluid is described in terms of density distribution functions $f_i(\mathbf{r}, t)$ giving the probability that a fictitious fluid particle with velocity $\mathbf{v}_i$ enters the lattice site $\mathbf{r}$ at discrete time t. The admissible velocities $\mathbf{v}_i$ are dependent on the lattice topology. Usually, i runs between 0 and z, where z is the lattice coordination number (i.e. the number of lattice links). By convention $\mathbf{v}_0 = 0$ and f_0 represents the density distribution of particles at rest. For many lattice topologies the set of vectors $\mathbf{v}_i$ can be divided in slow and fast velocities: slow velocities correspond to a jump to a nearest–neighbor site while fast velocities imply a jump to a second nearest–neighbor.

The dynamics we consider for the f_i's is given by the so-called BGK model[8,30]

$$f_i(\mathbf{r} + \Delta t \mathbf{v}_i, t + \Delta t) = \omega f_i^{(0)}(\mathbf{r}, t) + (1 - \omega) f_i(\mathbf{r}, t), \tag{1}$$

where Δt is the time step of the simulation, $\tau = 1/\omega$ a parameter called the relaxation time. The $f_i^{(0)}$'s are given function (called local equilibriums) which depend only on the fluid density $\rho = \sum_{i=0}^{z} m_i f_i$ and the fluid velocity $\mathbf{u}$ defined through the relation $\rho \mathbf{u} = \sum_{i=0}^{z} m_i f_i \mathbf{v}_i$. The quantities m_i are weights associated with the lattice directions and $m_0 = 1$ by definition.

It can be shown (see for instance, refs. 8 and 30) that Eq. (1) reproduces a hydrodynamical behavior if the local equilibrium functions are chosen as follows (Greek indices label the spatial coordinates and summation over repeated Greek indices is assumed)

$$f_i^{(0)} = \rho \left[\frac{1}{C_2} \frac{c_s^2}{v^2} + \frac{1}{C_2} \frac{\mathbf{v}_i \cdot \mathbf{u}}{v^2} + \frac{1}{2C_4 v^4} \left(v_{i\alpha} v_{i\beta} - v^2 \frac{C_4}{C_2} \delta_{\alpha\beta} \right) u_\alpha u_\beta \right],$$

$$f_0^{(0)} = \rho \left[1 - \frac{C_0}{C_2} \frac{c_s^2}{v^2} + \left(\frac{C_0}{2C_2} - \frac{C_2}{2C_4} \right) \frac{u^2}{v^2} \right].$$

Table I. **The geometrical coefficients necessary to compute the local equilibrium distributions in a LB simulation. The quantity v is the ratio of the lattice spacing to the time step dt and $m_0 = 1$ for all models**

Model	Slow velocities	Fast velocities	C_0	C_2	C_4
D1Q3	$|v_i| = v,\ m_i = 1$		2	2	2/3
D2Q9	$|v_i| = v,\ m_i = 4$	$|v_i| = \sqrt{2}v,\ m_i = 1$	20	12	4
D2Q7	$|v_i| = v,\ m_i = 1$		6	3	3/4
D3Q15	$|v_i| = v,\ m_i = 1$	$|v_i| = \sqrt{3}v,\ m_i = 1/8$	7	3	1
D3Q19	$|v_i| = v,\ m_i = 2$	$|v_i| = \sqrt{2}v,\ m_i = 1$	24	12	4

Table I gives the values of the coefficients C_k and the weight m_i for a few standard lattice topologies noted $DdQ(z+1)$, where d is the spatial dimension. The quantity v gives the speed unit. It corresponds to the modulus of the slow velocities. Note that the expression we propose here for the local equilibrium distribution is exactly equivalent to the standard one (see ref. 30). However, the formulation in terms of the topological coefficients C_0, C_2, and C_4 and weights m_i more clearly separates the topology issues from the physical aspects.

As mentioned earlier, Eq. (1) with (2) for the local equilibrium distributions is equivalent to the continuity equation and Navier–Stokes equation with speed of sound $c_s < v(C_2/C_0)$ and dynamic viscosity μ

$$\mu = \rho \frac{C_4}{C_2} \left(\frac{1}{\omega} - \frac{1}{2} \right) v^2 \, \Delta t. \tag{2}$$

A commonly chosen value for c_s is $c_s^2 = v^2(C_4/C_2)$. In order to insure a positive viscosity, we have the condition $\omega < 2$. Yet values close to 2 are often numerically unstable.

In a *LB* scheme, the stress tensor

$$\Pi_{\alpha\beta}^{(1)} = \sum_i m_i v_{i\alpha} v_{i\beta} (f_i - f_i^{(0)}) \tag{3}$$

is related to the strain rate tensor $S_{\alpha\beta} = \frac{1}{2}(\partial_\beta u_\alpha + \partial_\alpha u_\beta)$ as (see ref. 8)

$$S_{\alpha\beta} = -\frac{C_2}{2\rho \Delta t \tau_\mu v^2 C_4} \Pi_{\alpha\beta}^{(1)}, \tag{4}$$

where $\tau_\mu = 1/\omega$ is the relaxation time corresponding to the viscosity μ given by relation 2.

3. THE NON-NEWTONIAN MODEL

In the case of a non-Newtonian rheology, one expects that the viscosity μ also depends on the strain rate according to some phenomenological relation. In this case, Eq. (4) together with (2) must be solved for μ so as to satisfy the desired non-Newtonian shear-stress versus strain rate relation. In this section, we address this question in the case of the so-called Casson's Rheology Model.[14] Our goal is to show that the LB framework can describe hemodynamics beyond the Newtonian regime. As in previous works such as for instance,[2,28] we locally adjust the relaxation parameter ω as a function of the shear stress but here, in addition, we take into account the fact that the shear stress also depends on ω. Thus, we solve a consistency relation that was neglected in previous approaches.

3.1. Casson's Rheology Model

The Casson's model is only valid under specific conditions and should not be regarded as an exhaustive description of blood. Blood with small shear rates ($\dot{\gamma} \leqslant 10\,\mathrm{s}^{-1}$) and hematocrit less than 40%, can be described by Casson's equation (see ref. 14)

$$\sqrt{\eta|\dot{\gamma}|} = \begin{cases} \sqrt{\sigma} - \sqrt{\sigma_y} & \text{if } \sigma > \sigma_y, \\ 0 & \text{otherwise,} \end{cases} \tag{5}$$

where η is a constant viscosity, σ the shear stress, $|\dot{\gamma}|$ is the shear strain rate defined as $2|S_{\alpha\beta}|$ and σ_y is the so-called *yield stress*. This relation expresses the fact that below some stress σ_y, no strain rate is observed. The quantity σ_y is of the order of $0.05\,\mathrm{dyn/cm}^2$ and is almost independent of the temperature in the range 10–37° C. Without fibrinogen, a suspension of red cells has zero yield stress.

From Casson's model we also see that, at high shear rate, blood behaves like a Newtonian fluid in which $\sigma = \eta|\dot{\gamma}|$

It is a common practice to write Casson's model in the standard form

$$\sigma = \mu|\dot{\gamma}| \quad \text{where } \mu = \mu(|\dot{\gamma}|). \tag{6}$$

From Eq. (5), one obtains the following expression for μ as a function of the shear strain rate $\dot{\gamma}$

$$\mu = \begin{cases} \dfrac{(\sqrt{\sigma_y} + \sqrt{\eta|\dot{\gamma}|})^2}{|\dot{\gamma}|} & \text{for } \sigma > \sigma_y, \\ \infty & \text{for } \sigma \leqslant \sigma_y. \end{cases} \tag{7}$$

3.2. Case of a Channel Flow

Here we consider the stationary velocity profile resulting from Casson's rheology in the case of a cylindrical tube of radius a. The application of Stokes equation leads to[14]

$$\sqrt{\frac{-r}{2}\frac{dp}{dx}} = \sqrt{\sigma_y} + \sqrt{\eta}\sqrt{-\frac{du}{dr}}, \tag{8}$$

where r is the distance from the channel center. This equation leads to the definition of a critical radius r_c through the condition:

$$\frac{-dp}{dx} > \frac{2\sigma_y}{r} \quad \text{for } r_c < r < a. \tag{9}$$

The meaning is that, below the critical radius, the shear is not perceived.

Integrating Eq. (8) gives the following velocity profile[14]

$$u(r) = -\frac{1}{4\eta}\frac{dp}{dx}\begin{cases} a^2 - r^2 - \frac{8}{3}\sqrt{r_c}(\sqrt[3]{a^2} - \sqrt[3]{r^2}) + 2r_c(a-r) & \text{if } r \geqslant r_c, \\ (a^2 - \frac{8}{3}\sqrt{r_c}\sqrt[3]{a^2} + 2r_c a - \frac{1}{3}r_c^2) & \text{if } r \leqslant r_c. \end{cases} \tag{10}$$

Note that, in the Newtonian case, the *Poiseuille* velocity profile is equal to $u(r) = -\frac{1}{4\eta}(a^2 - r^2)(dp/dx)$.

3.3. LB Casson's Model

We shall now inject the above rheology model into the LB scheme. It can be shown that the results obtained in Section 2 are still valid when the relaxation time $\tau_\mu = 1/\omega$ depends on the strain rate, at least to first order in the Knudsen number.

The fundamental equations are (5), which by substituting $\sigma = \mu|\dot{\gamma}|$, can be rewritten as (for $\sigma > \sigma_y$)

$$|\dot{\gamma}| = \frac{\sigma_y}{(\sqrt{\mu} - \sqrt{\eta})^2} \tag{11}$$

and Eq. (4) which can be expressed as

$$|\dot{\gamma}| = 2\sqrt{S_{\alpha\beta}S_{\alpha\beta}} = \frac{C_2\sigma}{\tau_\mu v^2 C_4 \rho \Delta t}, \tag{12}$$

where the stress $\sigma = \sqrt{\Pi_{\alpha\beta}^{(1)}\Pi_{\alpha\beta}^{(1)}}$ is directly computed from the density distribution functions, as indicated in Eq. (3).

Since, from Eq. (2), $\tau_\mu = \left(\frac{C_2}{v^2 \rho C_4 \Delta t}\mu + \frac{1}{2}\right)$, Eqs. (11) and (12) must be solved for μ. After equating $|\dot{\gamma}|$ from both relations, one gets the condition

$$\frac{\sigma_y}{(\sqrt{\mu} - \sqrt{\eta})^2} = \frac{\sigma}{\mu - (\rho \Delta t v^2 C_4)/(2C_2)}. \tag{13}$$

The physically meaningful solution of this equation for μ is

$$\sqrt{\frac{\mu}{\eta}} = \frac{1}{1-\theta}\left[1 + \sqrt{\theta[1 + \frac{\rho \Delta t v^2}{\eta}\frac{C_4}{2C_2}(1-\theta)]}\right], \tag{14}$$

where $\theta = \sigma_y/\sigma$.

Equation (14) is valid when $\theta < 1$, i.e., when $\sigma > \sigma_y$. Otherwise, from Casson's rheology, we know that the viscosity is infinite. In the numerical model, however, we have introduced a ceiling viscosity μ_∞ for small shear stress values. This cutoff viscosity is reached when $\sigma = \sigma_y + \epsilon$ and remains constant for all the smaller values of the stress. The value of μ_∞ is obtained from Eq. (14) by taking $\theta = \sigma_y/(\sigma_y + \epsilon) \approx 1 - \epsilon/\sigma_y$. The choice of ϵ is, on the other hand, somehow arbitrary. Here we chose it so as to produce a relaxation time $\tau_\infty = 5$. We have checked numerically that a smaller value for ϵ no longer improves the velocity profile in the channel flow simulation.

Figure 1 plots the resulting value of $\sqrt{\mu/\eta}$ as a function of the possible values of θ. Here, no cutoff on the viscosity has been applied.

We now discuss a $D2Q9$ LB simulation in which the relaxation time $1/\omega = \tau_\mu$ is locally adjusted as a function of the local value of σ, in agreement with relation (14). The channel flow geometry has been considered because analytical solution 10 can be used to validate the non-Newtonian behavior.

The channel width L was set to 41 lattice sites, the yield shear stress σ_y was 10^{-6}, the characteristic Casson's width was $r_c = 0.01L$ and the driving force was 0.0001. The value of η in Eq. (5) was chosen so as to correspond to a relaxation time $\tau_\mu = 1$. The so-called full-way bounce-back[10,30] boundary condition has been imposed at the channel boundary.

The upper left panel in Fig. 2 shows that the u_x profile fits very well with the expected analytical profile of Eq. (10). The channel width is represented along the horizontal axis. The upper right panel shows the symmetry of the absolute value of the shear rate around the center of the tube.
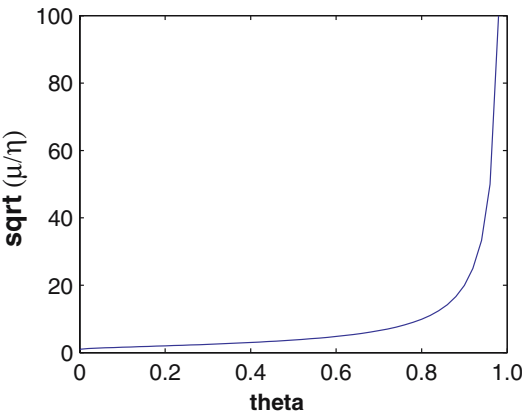
Fig. 1. The solution for the effective viscosity as a function of the shear stress, for $C_4/C_2 = 1/3$ and $\rho \Delta t v^2/\eta = 1$.
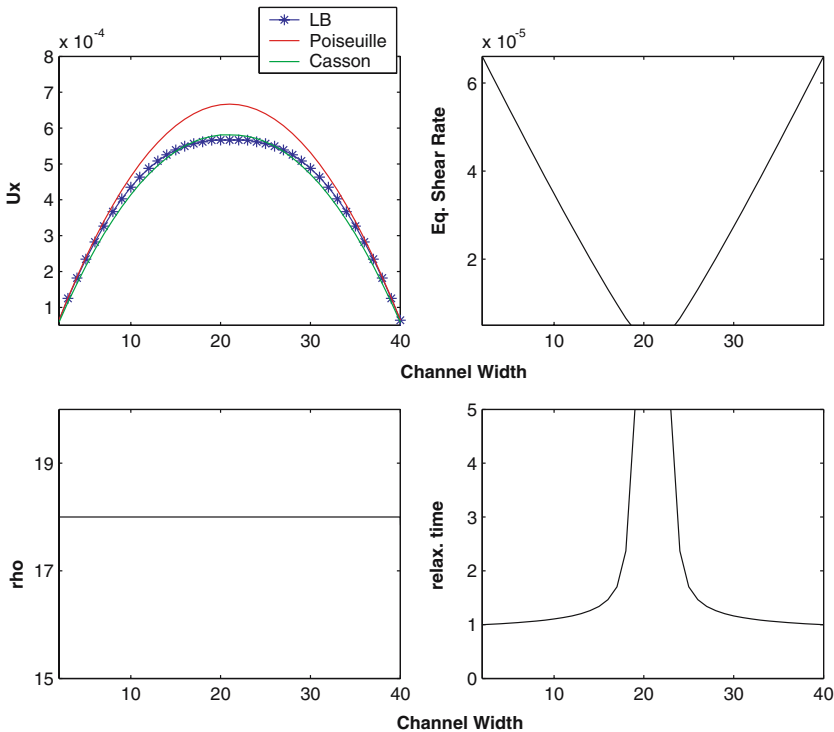

Fig. 2. Poiseuille and Casson's profiles are shown in the upper left panel. On the right of it, the shear rate is displayed. Down, from left to right, the density ρ and the relaxation time τ_μ are sketched.

The variation of the relaxation time τ_μ against the channel width is drawn in the lower right panel of the figure. At boundaries, τ_μ is close to 1, the imposed value for large stress, and at the center of the tube it grows up to its maximum artificially allowed value. The lower left panel shows that the density ρ is constant across the tube width.

4. THE THROMBOSIS MODEL

A blood clot, also called thrombus, consists of a plug of plate-lets enmeshed in a network of insoluble fibrin. It typically appears in low-shear stress regions and thus may depend on non-Newtonian prop-erties of bloodflow. Thrombosis stops the bleeding in the vessel through *hemostasis*, a complex cascade process involving the contribution of more than 20 proteins.[5] During the next stage, platelets aggregate and initiate a cascade of reactions which then accelerate the thrombosis formation and transforms a fragile soft clot into a stable hard clot in which the red blood cells (RBC) aggregate tightly in a network of stabilizing *fibrin* molecules.

Here, we describe a preliminary mesoscopic model of blood clotting. Thrombosis formation will be simulated in the *LB* approach by adding RBC as discrete point particles (suspensions) transported by the plasma. This process will be modeled according to the rules described in ref. 26 and extensively validated in refs. 11 and 12, in the case of a LB model for sediments transport and deposition. Note that here we want to con-sider a simple, mesoscopic description of RBC and we assume that they can be represented as passive scalars. Therefore, detailed models for col-loid suspensions such as that proposed by Ladd[22] or the more micro-scopic approach by Ahlrichs and Dünweg[3] are not approriate for the desired level of description and computational efficiency.

Note also that, in our approach, the intensity of non-Newtonian behavior described earlier in this paper, that is the value of the yield stress σ_y can be adjusted locally as a function of the RBC density, in accordance to what is observed for real blood. However, this feature has not yet been implemented.

A scenario which is commonly proposed for the clotting[20] is that RBC aggregation can take place at the vessel walls if the shear stress is smaller than some threshold (endothelium barrier). In a non-stented aneurysm, the shear stress at the wall is usually larger than this threshold. However, if the stent design is approriate, it will reduce the flow in the aneurysm and the shear stess at its wall, thus allowing clotting to start and grow.

To implement this idea in our model, we will allow the RBC to aggregate, as is described for instance in Reaction Limited Aggregation (RLA) or Diffusion Limited Aggregation (DLA) models[27] and to form a

growing thrombus. Here, the RBC aggregation will take place with some given probablitity only where the shear stress is low enough and near a boundary (either a wall or a forming clot). The implementation of such a growth mechanism in a LB model with passive scalars has been largely used in other applications where aggregation occurs (see for instance refs. 7 and 9). Note that, in the present model, the action of the platelets is simulated by setting the above aggregation probablitity as function of the shear stress.

Figure 3 illustrates the behavior of our model with and without stent, in a y-shaped geometry with an aneurysm. We clearly see that without the stent, clotting doesn't occur as the shear stress is too high at the wall, whereas, when the stent is inserted, a thrombus grows and fills in the aneurysm.

Obviously, the threshold value for the shear stress has been choosen arbitrarily in this example. The next step is the calibration and validation of this thrombosis engineering framework with respect to *in vivo* or *in vitro* clotting experiments.

Figure 4, left and right, shows the effects of the stent on the blood pressure and velocity at an intermediate stage before the thrombosis model operates. The pressure intensity in the aneurysm is displayed together with the velocity steamlines. The stent modifies the blood pressure and velocity profiles on both the vessels and the aneurysm. In particular, the pressure decreases dramatically in the small bleb area (at the upper-right part of the aneurysm) after stent placement. In addition, the vortices change direction in the neck area (anti-clockwise without stent and clock-wise with stent).
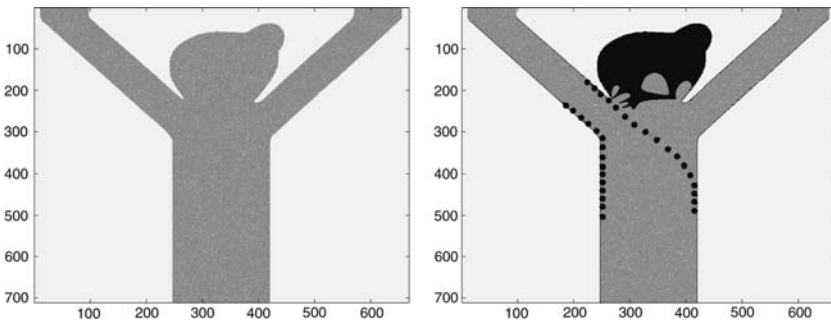

Fig. 3. Illustration of the clotting model in a non-stented (left) and stented (right) aneurysm that has grown in a y-shaped junction. The gray color indicate the region where blood flow occur. White dots indicate RBC's. The bige black dots displayed on the right panel indicate the struts of the stent. Without stent, the shear stress is too high to initiate clotting. The presence of a stent reduces the flow inside the aneurysm, thus activating the thrombosis formation. The forming clot is shown in the aneurysm as the black region on the right panel. Notice that the thrombus has formed in the aneurysm only, not in the vessels.
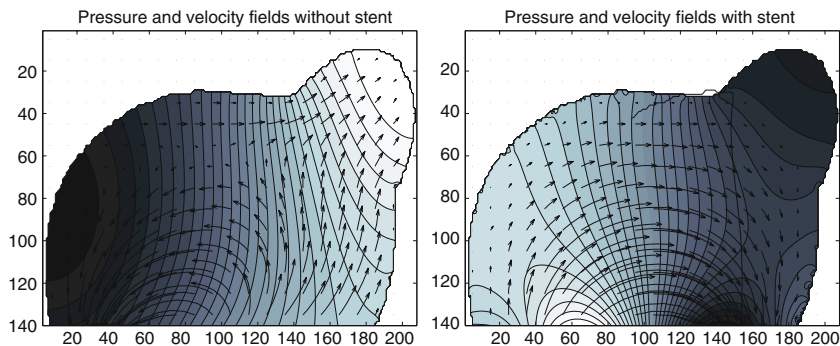
Fig. 4. Blood pressure and velocity field in the aneurysm, without stent (left) and with stent (right). The color levels show the intensity of the displayed quantites.
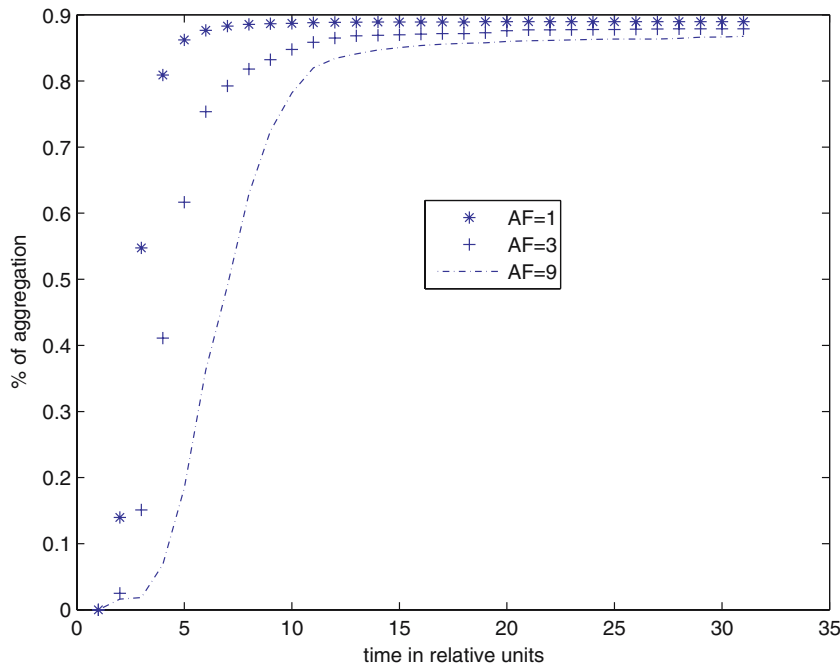

Fig. 5. Clotting dynamics (i.e aggregation fraction) in the aneurysm. The horizontal axis shows the iteration time and the vertical one represents the fraction of the aneurysm that has clot. The three different curves are produced with three different aggregation factors (AF), but the same shear stress threshold and same aggregation probability.

When the thrombosis model is activated, a clot start forming at the vessel wall where the shear stress is below some given threshold. Figure 5 shows in more detail the dynamics of the clotting process. First, there is an activation regime, then a growth regime which is linear with time and, finally a saturation phase reflecting the fact that the clot boundary has reached a flow region where the shear stress is above the chosen threshold. The speed of the process is related to the aggregation factor (i.e. the number of RBC needed to fill in a lattice cell) as illustrated by the different curves on Fig. 5.

It is interesting to notice the correspondance of the above behavior (activation, growth and saturation) with the high shear rate platelet aggregation and clotting process described in refs. 5 and 32.

5. CONCLUSION

This paper describes on going research addressing bloodflow simulations within the context of the LB approach. A realistic blood rheology model has been developed and validated in a simple case. Although still qualitative in nature, we have outlined how the flexibility of the LB method allows us to explicitly describe thrombosis formation in stented aneurysms.

ACKNOWLEDGMENTS

REFERENCES

1. M. Aenis, A. P. Stancampiano, A. K. Wakhloo, and B. B. Lieber, *ASME J. Biomed. Eng.* **119**:206 (1997).
2. E. Aharonov and D. H. Rothman, Non-newtonian flow (through porous media): a lattice boltzmann method. *Geophys. Res. Lett.* **20**:679–682 (1993).
3. P. Ahlrichs and D. Dünweg, Lattice boltzmann simulation of polymer-solvent system, *Int. J. Mod. Phys. C* **9**:1429 (1998).
4. A. M. M. Artoli, A. G. Hoekstra, and P. M. A. Sloot, *Lect. Notes Comput. Sci.* **2329**:361 (2002).
5. D. I. Ataullakhanov, V. I. Zarnitsina, A. V. Pokhilko, A. I. Lobanov, and O. L. Morozova, Spatio-temporal dynamics of blood coaggulation and pattern formation – a theoritical approach. *Int. J. Bifurc. Chaos*. **12**(9):1985–2002 (2002).
6. J. L. Berry, E. Manoach, C. Mekkaoui, P. H. Rolland, J. E. Moore, and A. Rachev, *J. Vasc. Interv. Radiol.* **13**:97 (2002).

7. B. Chopard and M. Droz, *Cellular Automata Modeling of Physical Systems* (Cambridge University Press, 1998).

8. B. Chopard, A. Dupuis, A. Masselot, and P. Luthi, *Adv. Complex Syst.* **2&3**:103–246 (2002).

9. B. Chopard, P. Luthi, and M. Droz, Reaction-diffusion cellular automata model for the formation of Liesegang patterns, *Phys. Rev. Lett.* **72**(9):1384–1387 (1994).

10. B. Chopard, P. Luthi, and A. Masselot, Cellular automata and lattice boltzmann techniques: An approach to model and simulate complex systems, 1998. http://cui.uni-ge.ch/~chopard/FTP/CA/advp.ps.gz.

11. B. Chopard, A. Masselot, and A. Dupuis, A lattice gas model for erosion and particles transport in a fluid. In *Proceedings of the LGA'99 conference, Tokyo*, Yu Chen *et al.*, ed. Vol. 129, pp. 167–176. Computer Physics Communications, 2000.

12. A. Dupuis and B. Chopard, Lattice gas modeling of scour formation under submarine pipelines, *J. Comp. Phys.* **178**:161–174 (2002).

13. H. Fang, Z. Wang, Z. Lin, and M. Liu, *Phy. Rev.* **E65**:051925 (2002).

14. Y. C. Fung, *Biomechanics: Mechanical Properites of Living Tissue* (Springer-Verlag, 1993).

15. G. Geremia, M. Haklin, and L. Brennecke, *AJNR Am. J. Neuroradiol.* **15**:1223 (1994).

16. ISAT Collaborative Group, *Lancet.* 1267–1274 (2002).

17. M. Hamuro, J. C. Palmaz, E. A. Sprague, C. Fuss, and J. Luo, *J. Vasc. Interv. Radiol.* **12**:607 (2001).

18. M. Hirabayashi, M. Ohta, D. A. Rüfenacht, and B. Chopard, *Phys. Rev.* **E68**:021918 (2003).

19. M. Hirabayashi, M. Ohta, D. A. Rfenacht, and B. Chopard, In *Lect. Notes Comput. Sci.* Vol. 2657, page 1044, 2003.

20. M. Hirabayashi, M. Ohta, D.A. Rfenacht, and B. Chopard, A lattice boltzmann study of blood flow in stented aneurysms. In *Future Generation Computer Systems (FGCS)*, Vol. 20, pp. 925–934, 2003.

21. S. G. Imbesi and C. W. Kerber, *AJNR Am. J. Neuroradiol.* **22**:721 (2001).

22. A. J. C. Ladd, Numerical simulation of particulate suspensions via a discretized boltz-mann equation, *J. Fluid Mech.* **271**:285,310 (1994).

23. B. B. Lieber, A. P. Stancampiano, and A. K. Wakhloo, *Ann. Biomed. Eng.* **25**(3):460–469 (1997).

24. T. M. Liou, W. C. Chang, and C. C. Liao, *Exp. Fluids.* **23**:317 (1997).

25. M. P. Marks, M. D. Dake, G. K. Steinberg, A. M. Norbash, and B. Lane, *Radiology* **191**:441 (1994).

26. A. Masselot and B. Chopard, A lattice boltzmann model for particle transport and deposition, *Europhys. Lett.* **42**:259–264 (1998).

27. P. Meakin, *Fractals, Scaling and Growth far From Equilibrium* (Cambridge University Press, 1998).

28. N. Rakotomalala, D. Salin, and P. Watzky, Simulations of viscous flows of complex fluids with a Bhatnagar, Gross, and Krook lattice gas, *Phys. Fluids.* **8**(11):3200–3202 (1996).

29. C. Sadasivan, B. B. Lieber, M. J. Gounis, D. K. Lopes, and L. N. Hopkins, *AJNR Am. J. Neuroradiol.* **23**:1214 (2002).

30. S. Succi, *The Lattice Boltzmann Equation, For Fluid Dynamics and Beyond* (Oxford University Press, 2001).

31. A. K. Wakhloo, F. Schellhammer, J. de Vries, J. Haberstroh, and M. Schumacher, *AJNR Am. J. Neuroradiol.* **15**:493 (1994).

32. D. M. Wootton, C. P. Markou, S. R. Hanson, and D. N. Ku, A mechanistic model of acute platelet accumulation in thrombogenic stenoses, *Ann. Biomed. Eng.* **29**:321–329 (2001).

33. S. C. M. Yu and J. B. Zhao, *Med. Eng. Phys.* **21**:133 (1999).